Arch. Metall. Mater. **69** (2024), 3, 1097-1106

DOI: https://doi.org/10.24425/amm.2024.150930

Z. BELAMRI[1*], L. CHETIBI[1,2]

SYNTHESIS OF SUPERHYDROPHOBIC METAL COATING BASED ON NANOSTRUCTURED ZnO THIN FILMS IN ONE STEP: EFFECT OF SOLVENTS

In this work, ZnO thin film is prepared by spraying a solution of zinc acetate precursor prepared with different solvents, namely, methanol, ethanol and distilled water at optimized conditions for aluminum substrate temperature and solution concentration. The impact of different solvents on the structural and hydrophobic properties of ZnO thin films was investigated by X-ray diffraction, Raman spectroscopy, Field Emission Scanning Electron Microscope and a Profilometer-Roughness Tester. The morphology of the elaborated ZnO thin films is spherical shaped nanostructured decorated by textures such as bumps (coexistence of ZnO micro-nanostructures). The results confirm that the different solvents used to prepare the ZnO thin films have a significant impact on the characteristics of these layers and the wettability study reveals that the surface of ZnO thin film prepared with distilled water is superhydrophobic.

Keywords: Superhydrophobic; nanostructures; one step; contact angle; ZnO thin film

1. Introduction

Wettability, which has to do with a surface's affinity for water, is the most crucial property of the material surface. It is generally accepted that a surface's wettability is primarily influenced by its surface energy, surface roughness, or surface micro-nanostructure. Hydrophobicity is a parameter that expresses the wettability of a surface which is highly influenced by surface properties, like chemical composition, structure morphology, and the contact angle (CA) of the liquid with these surfaces, each surface can be classified into different domains, such as superhydrophilic (CA = 5° in 0.5 sec), hydrophilic (CA = 90°), hydrophobic (CA > 90°), and superhydrophobic (CA = 150°-180°) [1-11]. Superhydrophobicity is a property that describes the non-wetting characteristics of material surfaces. Several research works have been carried out for the preparation of such surfaces inspired by nature (ex. the inherent water repellent properties of lotus leaf surfaces). It can be carried out in two ways: the first is to create a rough hydrophobic surface and the second to modify this rough surface by compounds with low surface free energy, such as fluorinated or silicon compounds [12-17]. There are several applications of superhydrophobic coating on metallic materials; it can be used for satellite antenna, billboards and high-voltage line because it has good self-cleaning properties [18], anti-adherence of snow or ice, windows, etc. [19-21]. In this context, steel, copper, and aluminum are among the metals that are often used in daily life and in industrial applications due to their superior mechanical and physicochemical properties. The metal, however, is quickly corroded in the environment as a result of chemical or electrochemical interactions that cause the metal to become oxidized or ionic on its surface. It is known that corrosion is the physicochemical interaction between a metal and its environment, which results in changes in its surface properties [22]. The formation of a coating of passivation is one of the best techniques to stop corrosion on metal surfaces. So, the concept of superhydrophobic surface preparation creates enormous opportunities in the field of corrosion inhibition for metals and alloys. Due to their self-cleaning property and water roll-off performance, superhydrophobic coatings offer an approach to slow the breakdown of the metals oxide layer and thus prevent the metal surfaces below from corrosion [23].

Aluminum, especially, has been a crucial material for research in recent times due to its abundance in nature, ease of handling, and numerous industrial applications, particularly

[1] FRÈRES MENTOURI CONSTANTINE 1 UNIVERSITY, FACULTY OF EXACT SCIENCES, DEPARTMENT OF PHYSICS, LABORATORY OF PHASE TRANSFORMATIONS, CONSTANTINE 25000, ALGERIA
[2] ECOLE NATIONALE POLYTECHNIQUE DE CONSTANTINE, LABORATORY OF ADVANCED MATERIALS TECHNOLOGY, CONSTANTINE 25000, ALGERIA
* Corresponding author: belamri.zehira@umc.edu.dz

in the aerospace and local industries [24,25]. The fact that aluminum corrodes readily, particularly in aqueous environments with Cl^- ions, small quantities of Cl^- is a significant disadvantage for these applications [26]. So, it is necessary to fabricate superhydrophobic coating on this material. The use of super-hydrophobic coating has been shown to be an effective corrosion prevention technique in earlier studies [27]. The creation of a stable superhydrophobic coating which maintains long-term stability and excellent corrosion resistance property can be widely applied in the corrosion protection of various engineering components [18]. Due to their water-shedding properties, zinc superhydrophobic surfaces are ideal for anti-corrosion and anti-fog applications for metal structures and buildings [28].

By using zinc oxide (ZnO) nanoparticles suspended in alcohols at different bath temperatures and functionalized with stearic acid, superhydrophobic thin films have been created on aluminum alloy substrates using electrophoretic deposition [29]. The authors demonstrate how the deposited bath temperature increases with the thin-film roughness, water contact angle, and Zn:O atomic percentage. The same authors used electrodeposition of copper on aluminum surfaces and electrochemical modification with organic molecules containing stearic acid to generate superhydrophobic aluminum surfaces in another study [30]. A superhydrophobic coating with a high contact angle (158°) and a low sliding angle (2°) was fabricated by spraying a mixture of poly (methyl methacrylate) (PMMA) and hydrophobic silica nanoparticles (SNs) onto the steel surface by Pan et al. [31]. Measurements by Tafel extrapolation give a lower I_{corr}, a higher E_{corr}, and a higher R_p, which leads to better corrosion resistance. These characteristics correspond to coated steel much better than bare steel.

A recent study carried out by Hassan et al. [32] focus on the development of superhydrophobic surfaces using magnesium nanoparticles for catalytic applications. Through the use of etching, immersion, and annealing techniques, an excellent surface superhydrophobic was achieved on the aluminum substrate along with a high water contact angle of 160° and a low sliding angle of 2°. Rafael et al. [33] use a variety of techniques to create a low-cost superhydrophobic coating on 5052 aluminum alloy. They are able to produce superhydrophobic coatings with 164° contact and 1° slide angles. Surface modification and the addition of corrosion inhibitors are costly and, in some cases, take a long time, and they may cause toxicity and environmental problems. Therefore, it's critical to create easy, inexpensive, non-toxic, and ecologically friendly surface treatment techniques to stop metal corrosion. In our recent work, the fabrication of hydrophobic ZnO coatings on aluminum substrates was easily realized by the thermal oxidation of electroplating Zn thin layers. We have shown the effect of the oxidation time or temperature on the morphological and structural characteristics of the obtained ZnO thin films, which in turn affects the hydrophobicity of the ZnO coating [34,35].

In the present study, the fabrication of a superhydrophobic ZnO thin film with nanometric structure on the aluminum substrate is achieved using an easy process with a simple precursor and non-toxic chemicals in one step, compared to the others complex steps mentioned above, where we followed the solvent effect on this property. ZnO was chosen in the present work due to its unique properties, such as its abundance, non-toxicity of its elements, and high stability at room temperature.

2. Experiment

The spray pyrolysis technique was used to deposit ZnO nanoparticles as a thin film on the aluminum substrate. Before the deposition, the substrate undergoes mechanical polishing until a flat shape and a thickness of 2 mm are obtained. After that, it is ultrasonically cleaned for 15 minutes in two baths, one with distilled water and the other with ethanol.

To make a solution, 1,755 g of dehydrated zinc acetate ($Zn(CH_3COO)_2$-$2H_2O$) precursors were dissolved in three solvents: distilled water, ethanol and methanol (0,2 M). Acetic acid (CH_3COOH) was used as the complexing agent. The substrate temperature was fixed at 350°C.

The current phases and their orientations were investigated using a PANALYTICAL empyrean diffractometer (XRD, λ_{Cu} = 1,540 Å). The Raman spectra were measured on a HORIBA LabRAM HR Evolution spectrometer at room temperature with a monochromatic light source of 473 nm. The morphological and elemental analyses were performed using a Field Emission Gun Scanning Electron Microscope (FEG-SEM, Jeol FEG JSM-7100 F) equipped with an Energy Dispersive X-ray spectrometer (EDX). The thickness and roughness of studied ZnO films were performed by a Profilometer-Roughness Tester PCE-RT 1200. The surface wettability of ZnO thin films has been identified through the measurement of the water contact angle (WCA (Θ)) using an optical system composed of a lamp delivering white light for lighting and projecting the image of the drop deposited on the sample (LEYBOLD type light source (6 V, 30 W)) and a projection lens allowing the enlargement of the image of the drop projected on a translucent screen of dimension (30×30 cm^2).

3. Results and discussions

3.1. Structural studies

Fig. 1 shows the X-ray diffraction spectra of the elaborated ZnO thin films using the different solvents, which exhibits different peaks that correspond to the ZnO hexagonal Wurtzite structure (JCPDS file number: 01-070-2551). In addition, the obtained diffractograms have revealed a sharp and intense dominant peak indexed (002), which reveals that the preferential orientation of the studied sample is along the [002] direction. The peak intensities are more pronounced for ZnO thin film prepared with distilled water (ZnO-water), which means their best crystallinity.

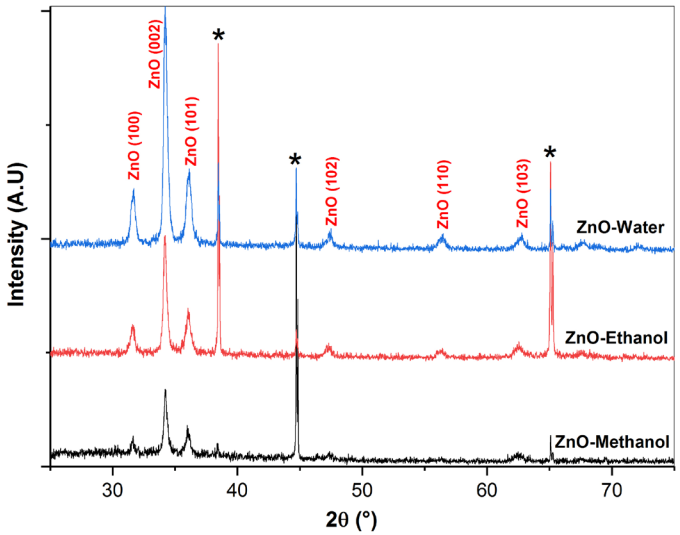

Fig. 1. X-ray spectra of prepared ZnO thin films using different solvent synthesized by spray pyrolysis (*: Al)

Crystalline size can be estimated by using the full width at half maximum of the (002) peak using the Scherrer method [36-39]:

$$D = \frac{0.9\lambda}{\beta \cos\theta} \tag{1}$$

Where: λ, θ and β are the X-ray wavelength (0.1540 nm), Bragg diffraction angle, and FWHM, respectively. TABLE 1 summarizes position (002) peak and estimated grain sizes.

The obtained results reveal that the average crystallite size is on the nanometric scale for all prepared samples (TABLE 1). The ZnO – water sample has larger crystallite sizes than the others, followed by the nanostructure obtained with the ethanol and methanol solvents (ZnO-etnol and ZnO-methanol). This difference can be linked to the difference of boiling points (T_b^{water} = 100°C, $T_b^{eth.}$ = 78. 24°C, and $T_b^{meth.}$ = 64.70°C) [40], and the viscosity of the used solvents; when larger crystallites are produced by solvent with higher viscosity and boiling temperature [41-43]. The highest viscosity can reduce the diffusion of ions in the solution leading to the formation of grouped crystallites with larger size [44].

The lattice parameters (a and c) can be calculated using the following relations valid for the hexagonal structure [45,46]:

$$a = \frac{\lambda}{\sin\theta\sqrt{3}} \tag{2}$$

$$c = \frac{\lambda}{\sin\theta} \tag{3}$$

$$\frac{1}{d_{hkl}^2} = \frac{4}{3}\left(\frac{h^2 + hk + k^2}{a^2}\right) + \frac{l^2}{c^2} \tag{4}$$

$$2d_{hkl}\sin(\theta_{hkl}) = n\lambda \tag{5}$$

Where: λ: wavelength of the X-ray used (0,1540 nm), θ: diffraction angle of the peak (100) for the parameter a and of the peak (002) for c, d_{hkl}: interreticular distance

The lattice parameters calculated for the elaborated ZnO thin films in this present work are different from those of the normalized ZnO (a = 0, 3490 nm and c = 0, 5207 nm). This indicates that the layer is stretched parallel to the growth direction; this may be due to the difference in the thermal expansion coefficients between the ZnO and the substrate [45]. It is known that the expansion coefficient α of aluminum substrate is 23×10^{-6}°C^{-1}. While ZnO has a hexagonal structure, its expansion coefficients α_{11} and α_{33} at room temperature are 6.05×10^{-6}°C^{-1} and $3{,}53\times10^{-6}$°C^{-1} respectively [45]. Consequently, this thermal maladjustment generates stresses in the deposited layer. When the crystal lattices of the substrate and the layer perfectly accommodate each other, a crystallographic relationship can appear at the interface. A deformation due to a disagreement between the lattice parameters of both materials can also be caused by this accommodation. As a result of this type of deformation, coherence stresses are generated in the two contacting materials. The state of stress in a ZnO thin film can be determined using an X-ray diffractogram. The biaxial stress e_{zz} along the c-axis direction perpendicular to the substrate is calculated from the following relationship [47,48]:

$$e_{zz}(\%) = \frac{C_{film} - C_0}{C_0} \times 100 \tag{6}$$

Where c_{film} and c_0 are the deposited layer and unconstrained layer lattice parameters, respectively (c_0 = 0, 5207 nm). The sign of the e_{zz} parameter confirms the type of stress that the layer experiences. In this present work, the value of e_{zz} represented in TABLE 1 is a positive sign, which confirms that this layer undergoes a tensile stress parallel to the layer growth direction. The residual stress σ parallel to the surface of the layer is expressed as follows [47,48]:

$$\sigma = \frac{2C_{13}^2 - C_{33}(C_{11} + C_{12})}{2C_{13}} \times \frac{C_{film} - C_0}{C_0} \tag{7}$$

With c_{ij} is the elastic constant for a monocrystalline structure of ZnO (c_{13} = 104,2 GPa, c_{33} = 213,8 GPa, c_{11} = 208,8 GPa and c_{12} = 119,7 GPa [47]).

$$\sigma\,(\text{GPa}) = -233 \times e_{zz} \tag{8}$$

TABLE 1

Values of D, a, c, e_{zz} and σ as a function of solvent type for elaborated ZnO thin films

Type of solvent	2θ (°)	FWHM (°)	Average crystallites sizes D (nm)	a (nm)	c (nm)	e_{zz} (%)	σ (GPa)
Distilled water	34.1483	0.1279	65	0.3294	0.5247	0.7704	–1.7949
Ethanol	34.1774	0.2047	41	0.3027	0.5243	0.6871	–1.3635
Methanol	34.2131	0.2558	32	0.3024	0.5237	0.5852	0.0358

According to the previous relations, it's found that there is a relation between the biaxial stress e_{zz} and the residual stress σ: they have the opposite direction in the plane of the interface between the layer and the substrate [45]. The calculated σ values of studied samples are presented in TABLE 1. They have a negative sign, indicating that the ZnO layers are under compressive force perpendicular to the c axis.

For a better evaluation of the ZnO film quality state, the calculation of other structural parameters is also necessary, in particular the dislocation density (δ) and the lattice strain (ε) using the following relations, Eq. 9 and Eq. 10 respectively [49]. TABLE 2 displays the calculated results obtained for these two parameters δ and ε.

$$\delta = \frac{1}{D^2} \tag{9}$$

$$\varepsilon = \frac{\beta \cos\theta}{4} \tag{10}$$

D is the average crystallite size.

TABLE 2

Structural parameters of ZnO thin film as function of solvent type

Type of solvent	2θ (°)	Average crystallites size D (nm)	Dislocation density ($\delta \times 10^{14}$ ligne/m^2)	Lattice deformation ($\varepsilon \times 10^{-3}$)
Distilled water	34.1483	65	2.37	0.53
Ethanol	34.1774	41	6.07	0.85
Methanol	34.2131	32	9.47	1.07

The found results show that a low value of (δ) is obtained for ZnO thin films prepared with distilled water, which indicates the presence of fewer defects in the deposited ZnO thin film, which leads to the best crystallization of the ZnO hexagonal phase. The increase in the crystallite size of this film is the origin of the decrease in stress.

The lattice strain (ε) is mainly due to the lattice shift between the film and the aluminum substrate. The minimum value of (ε) obtained for ZnO thin films prepared with distilled water indicates very little lattice mismatch between the substrate and the deposited film, with fewer defects in the elaborated ZnO thin film. It's known that water is less volatile compared to alcoholic solvents, so there is less possibility of complete evaporation of these solvents before reaching the substrate during the spraying process. This can decrease the lattice strain for the ZnO-water thin film. More explanations are exposed in the present work concerning this point in the morphological study section.

Fig. 2 shows the Raman spectra of the ZnO thin films synthesized by the spray pyrolysis technique. The prominent peak around 445 cm^{-1} observed for ZnO-water and ZnO-methanol samples is the characteristic peak of the Raman active principal mode E_2 (high) of Wurtzite ZnO [50-53]. This proves that ZnO thin films obtained with these two solvents have the Wurtzite hexagonal structure and that they crystallized greatly. Other peaks were observed on the Raman scattering spectra of these thin films (Fig. 2): the E_2 (Low) peak appears at 101 cm^{-1}, associated with the lattice vibration of the zinc atoms. The peak appears around 335 cm^{-1} with low intensity attributed to the (E_2 high-E_2 Low) mode which is the 2nd order characteristic caused by the multiphonon process [50]. The peak appears around 584 cm^{-1}, corresponding to the E_1 (LO) modes, which is a Raman-active vibrational mode of hexagonal Wurtzite ZnO, caused by impurities and defects such as oxygen vacancies [50,54]. For ZnO thin film prepared with ethanol, only two peaks corresponding to E_2 (high) and E_1 (LO) mode with low intensity are observed.

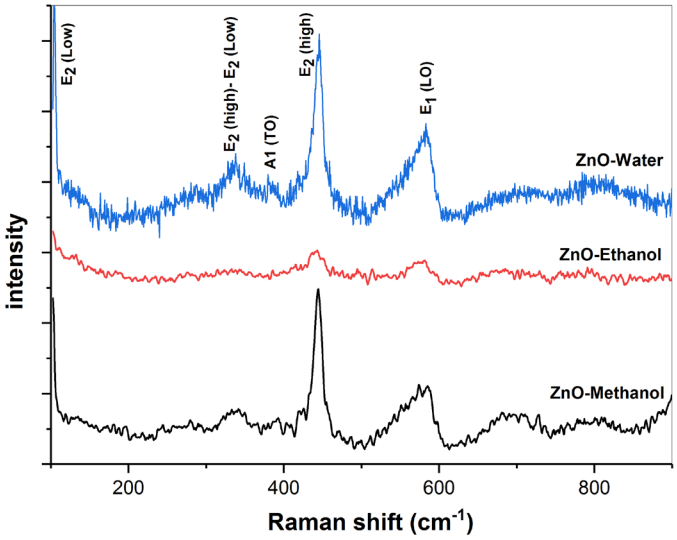

Fig. 2. Raman spectra of ZnO thin films using different solvent synthesized by spray pyrolysis

3.2. Morphological characteristics

The surface morphology of thin film has a significant impact on their superhydrophobic properties. Field Emission Gun Scanning Electron Microscope (FEG-SEM) observation (Fig. 3) shows the coexistence of ZnO micro-nanostructures, where a repeated distribution of the spherical nanostructures with grain sizes around 100 nm (inset image in Fig. 3 (a)) is decorated by textures such as bumps on the surfaces of the ZnO-water and ZnO-ethanol. The ZnO-water sample presents the largest bumps, approximately 10 µm (Fig. 3 (a)), compared to the ZnO-ethanol sample, which exhibits a greater density of small bumps of 3 µm (Fig. 3 (c)). However, the ZnO-methanol sample exposes an irregular shapes structure cover the film surface. The largest grain size revealed by the film prepared using water solvent can be linked to the higher viscosity of water compared with ethanol and methanol. By means of FEG-SEM observation, the distance between bumps (nearest neighboring particles) is different from solvent to another (Fig. 3(a), and (c)). The presence of zinc (Zn) and oxygen (O) in these thin films is confirmed by EDX analysis (Figs. 3(b), (d), (f)).

In light of previous studies, the explanation of the observed microstructure of the studied samples is expected from nature.

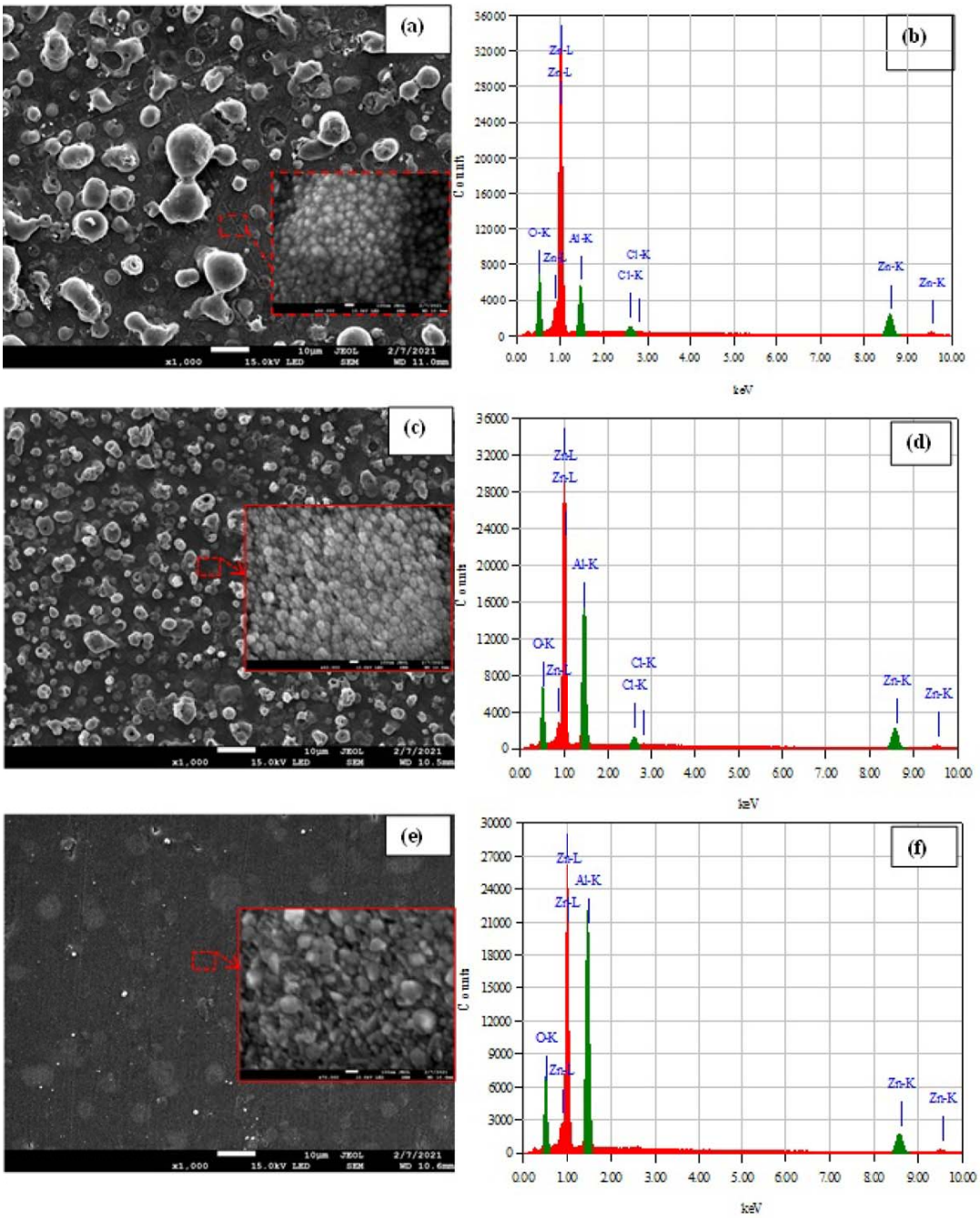

Fig. 3. FESEM images for ZnO thin films synthesized by spray pyrolysis (inset image shows the ZnO nanostructure distribution between ZnO bumps): (a) ZnO-Water; (c) ZnO-Ethanol; (e) ZnO-Methanol; (b) (d), (f) corresponding EDX spectra

Many plants and animals also have microtextures on their surfaces. It is frequent to notice the micro-sized bumps on plant leaves. These papillae are covered in fine nanostructures in several of these hydrophobic plants, including the lotus, which is the most well-known. The presence of two roughness scales significantly enhances the superhydrophobicity's quality [55-58]. This hierarchical structure, which is not required to obtain extremely high degrees of hydrophobicity, is nevertheless, poorly understood despite a plethora of intriguing theories [59]. A rice leaf is one example of a material where wetting and adhesion can be anisotropic due to the anisotropic arrangement of papillae at the surface [60]. Water will flow preferentially along specific paths on such materials.

From the obtained results, it is found that the three solvents used to prepare the ZnO thin films have a significant effect on the thickness of the studied samples. The cross-section FEG-SEM images of ZnO thin films (ZnO-water, ZnO-ethanol, and ZnO-methanol) are given in Fig. 4 and show the difference in layer thickness. TABLE 3 shows the thickness values obtained from Profilometer measurements, which range between 5 and 13 µm. This variation can be linked to the solvent volatility; methanol and ethanol have weak bonds, which increase their volatility compared to water. The low value of the thickness in ZnO-ethanol or ZnO-methanol films could be attributed to the evaporation of the solvent before reaching the substrate surface. The results are in agreement with the DRX analysis; the ZnO-water sample

shows the largest crystallite size with the largest thickness, which can be related to the increase of the (002) peak intensity in the X-ray diffraction spectrum. The films with lower thickness tend to grow with less favored orientation. Such observations are consistent with the decreasing FWHM of this peak. We can say that the crystallization degree is improved with thickness because increasing thickness has improved the mobility of the deposited atoms [61]. As more solute reaches the substrate's surface to create a film, there is a greater chance that more solutes will be attracted to one another to form a crystallite because of the increased electrostatic interaction between solute atoms [62]. Larger crystallites are created when the film thickens because more solute is gathered [63]. On another hand, from TABLE 2, the lattice strain and the dislocation density of studied ZnO thin films decrease with increasing thickness. It is possible to explain the decrease in lattice defects as crystallite increases in the presence of sufficiently thicker films in a less strained or more relaxed condition. As the size of the crystallites increases, the lattice strain and dislocation density decrease, indicating an improvement in crystallinity and a decrease in defects in the films [64].

TABLE 3

Values of crystallites size, Roughness, thickness, and contact angle as a function of solvent type

Type of solvent	Average crystallites size *D* (nm)	Roughness (µm)	Thickness (µm)	Contact angle (°)
Distilled water	65	0.172	13	156.00
Ethanol	41	0.132	6	143.50
Methanol	32	0.098	5	104.85

3.3. Wettability studies

Wettability involves the interaction between a liquid and a solid in contact. It is known that the wettability of an ideal surface, expressed by the contact angle (CA) of water droplets, is given by Young's equation [1]:

$$\cos\theta = \frac{\left(\lambda_{SV} - \lambda_{SL}\right)}{\lambda_{LV}} \tag{11}$$

Where θ = Young's contact angle on an ideal surface, and γ_{LV}, γ_{SV} and γ_{SL} refer to the liquid/vapour, solid/vapour and solid/liquid interfacial tensions, respectively. Fig. 6 shows a water drop with an almost specific shape on the surface of ZnO thin films synthesized in this work with different solvents. The value of the contact angle increases with increasing solvent viscosity, and the highest value (156°) is obtained in a ZnO thin film prepared with distilled water.

It is well-known that the surface energy, surface roughness, topography, surface micronanostructure, and chemical composition all play major roles in a surface's wettability [65-67]. As previously indicated, the state of the surface of the sprayed sample ZnO-water (Fig. 5 (b)) shows the coexistence of micronanostructure (ZnO bumps). The surface roughness of studied

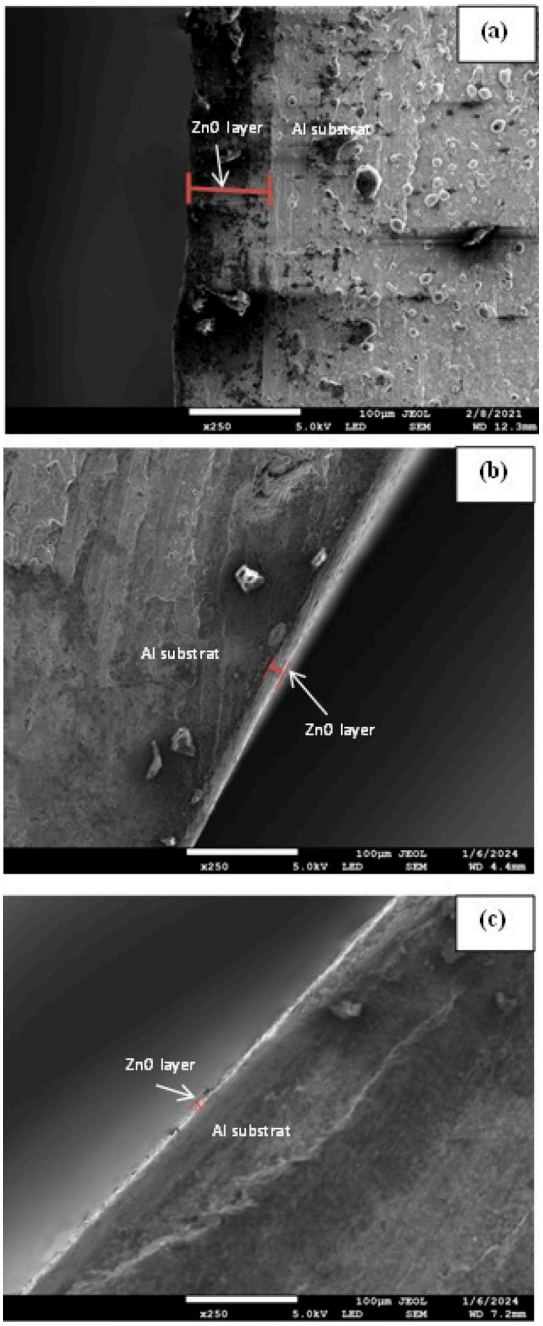

Fig. 4. FEG-SEM cross-section image for ZnO-water (a); ZnO-ethanol (b); ZnO-methanol (c)

samples increases from 0.098 µm to 0.172 µm when the films thickness increased from 5 µm to 13 µm, accompanied by an increase in contact angle (TEBLE 3). This may be due to the increased size and density of the ZnO bumps. As discussed above, solvents with a faster rate of evaporation leads to surface with a lower surface roughness due to the appearance of separated clusters. Ethanol and methanol have a high evaporation rate, which lead to the few of these clusters since the rapidly evaporating solvent leaves little time for surface mobility or diffusion of the molecules on the substrate. This traduce by results in lower aggregation and films with a non-coalesced morphology [68].

Increased surface roughness within a specific size range has been shown to improve wettability [69] because the air trapped

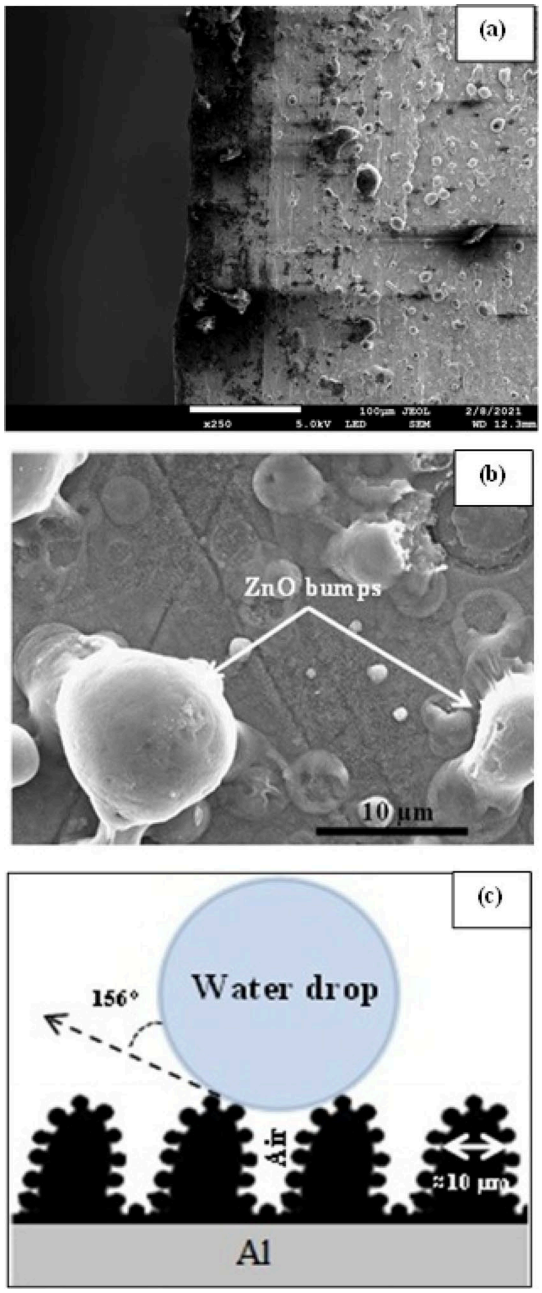

Fig. 5. (a) FEG-SEM cross-section image for ZnO-Water thin film; (b) FEG-SEM image shows ZnO bumps in ZnO-Water sample; (c) Schematic representation of the interface between a superhydrophobic surface and a water drop

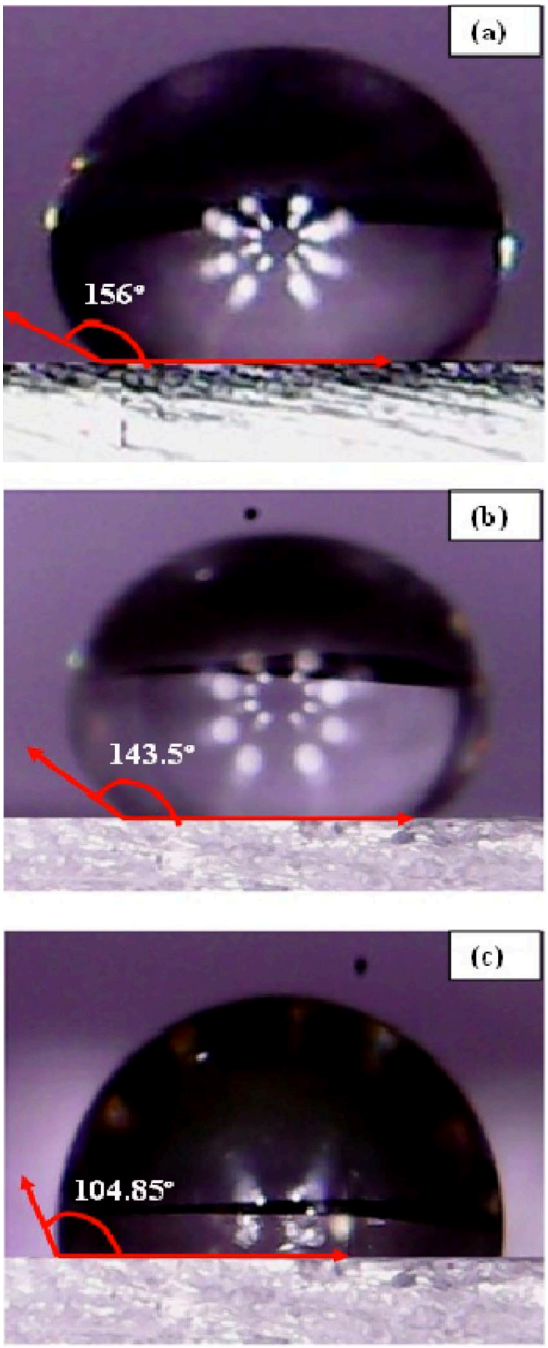

Fig. 6. Form of water drop on surface of ZnO thin films elaborated from different solvent: (a) ZnO-Water; (b) ZnO-Ethanol; (c) ZnO-Methanol

between solid surfaces and water droplets might reduce the contact area. Hence, the most promising structures for reaching the superhydrophobic surfaces are those that exhibit roughness on both the micro- and nanoscales a term known as "micronanobinary structures" [69]. The coexistence of surface roughness (micro-nanostructure) and low surface energy coating is crucial for surfaces that exhibit superhydrophobicity, as highlighted by a number of previously published works on superhydrophobic surfaces made using water [70,71]. The idea of the roughness effect on the contact angle has been studied where liquid does not penetrate the trough on a rough surface and leaves air gaps [72], as presented on Fig. 5(c), the formation of the bumps on the surface traps air on this surface and prevents water from adhering to the ZnO film, which leads to the superhydrophobicity of the material. Additionally, the presence of nanostructures can trap air between them, resulting in air pockets on the surface that inhibit the diffusion of water.

The superhydrophobic surface structure can be visualized as the hills and valleys (Fig. 5(c)) exhibiting micro-nano topography [73]. The air trapped in the "valleys" can prevent corrosive fluids, from effectively reaching the stripped surface, thus providing good protection against corrosion. According to Laplace's physical principle and pressure, when a vertical cylindrical tube is placed in a liquid, the liquid rises and forms

a concave surface called a meniscus if the tube is hydrophilic; otherwise, the liquid is lowered if the tube is hydrophobic [73]. Corrosive media tend to be expelled from the pores of superhydrophobic films. Therefore, this quality contributes to its anti-corrosion properties.

4. Conclusion

Finally, the superhydrophobic ZnO thin film was successfully deposited on the aluminum substrate at 350°C using a low-cost spray pyrolysis technique that requires no high temperature annealing. The obtained results show that the different solvents used to prepare the ZnO thin films have a significant impact on the characteristics of these layers. Structural analysis confirms that ZnO thin film has a hexagonal Wurtzite crystal structure, is polycrystalline, and has (002) preferential orientation. FEG-SEM observation confirms the coexistence of ZnO micro-nanostructure. The increase of roughness and thickness of the coating caused an increase in the contact angle. The reason for this was that more ZnO particles were deposited with thicker coatings. ZnO's function was to confine liquid to the surface, resulting in less material-liquid interaction. Consequently, the quantity of ZnO depositions affected the material's superhydrophobic properties. The studied thin films can be used to limit the presence of water and frost in the automotive and aeronautical fields.

Acknowledgements

The author warmly thank Prof. D. HAMANA, director of National Polytechnic School of Constantine (ENPC), Algeria, for her precious help and support.

REFERENCES

[1] K. Manoharan, B. Shantanu, Superhydrophobic surfaces review: Functional application, fabrication techniques and limitations. J. Micromanuf. **2**, 1, 59-78 (2019). DOI: https://doi.org/10.1177/2516598419836345

[2] H. Gau, S. Herminghaus, P. Lenz, R. Lipowsky, Liquid morphologies on structured surfaces: from microchannels to microchips. Science **283**, 46-49 (1999). DOI: https://doi.org/10.1126/science.283.5398.46

[3] N. Labbortt, J.P. Folkers, G.M Whitesides, Manipulation of the wettability of surfaces on the 0.1-to 1-micrometer scale through micromachining and molecular self-assembly. Science **257**, 1380-1382 (1992). DOI: https://doi.org/10.1126/science.257.5075.1380

[4] P. Lenz, Wetting Phenomena on Structured Surfaces. AdV. Mater. **11**, 18, 1531-1534 (1999). DOI: https://doi.org/10.1002/(SICI)1521-4095(199912)11:18<1531:AID-ADMA1531>3.0.CO;2-U

[5] S. Abbott, J. Ralston, G. Reynolds, R. Hayes, Reversible Wettability of Photoresponsive Pyrimidine-Coated Surfaces. Langmuir **15**, 26, 8923-8928 (1999). DOI: https://doi.org/10.1021/la990558o

[6] D. Yoo, S.S. Shiratori, M.F. Rubber, Controlling Bilayer Composition and Surface Wettability of Sequentially Adsorbed Multilayers of Weak Polyelectrolytes. Macromolecules **31**, 1, 4309-4318 (1998). DOI: https://doi.org/10.1021/ma9800360

[7] L. Jiang, R. Wang, B. Yang, T.J. Li, D.A. Tryk, A. Fujishima, K. Hashimoto, D.B. Zhu, Binary cooperative complementary nanoscale interfacial materials. Pure Appl. Chem. **72**, 1-2, 73-77 (2009). DOI: https://doi.org/10.1351/pac200072010073

[8] M.H. Hui, M.J. Blunt, Effects of Wettability on Three-Phase Flow in Porous Media. J. Phys. Chem. B **104**, 16, 3833-3845 (2000). DOI: https://doi.org//10.1021/jp9933222

[9] W. Chen, A.Y. Fadeev, M.C. Hsieh, D. Oner, J. Youngblood, T.J. McCarthy, Ultrahydrophobic and Ultralyophobic Surfaces: Some Comments and Examples. Langmuir **15**, 10, 3395-3399 (1999). DOI: https://doi.org/10.1021/la990074s

[10] J.P. Youngblood, T.J. McCarthy, Ultrahydrophobic, Polymer Surfaces Prepared by Simultaneous Ablation of Polypropylene and Sputtering of Poly(tetrafluoroethylene) Using Radio Frequency Plasma. Macromolecules **32**, 20, 6800-6806 (1999). DOI: https://doi.org/10.1021/ma9903456

[11] D. Oner, T. J. McCarthy, Ultrahydrophobic Surfaces. Effects of Topography Length Scales on Wettability. Langmuir **16**, 20, 7777-7782 (2000). DOI: https://doi.org/10.1021/la000598o

[12] A. Nakajima, A. Fujishima, K. Hashimoto, T. Watanabe, Preparation of Transparent Superhydrophobic Boehmite and Silica Films by Sublimation of Aluminum Acetylacetonate. AdV. Mater. 11, 16, 1365-1368 (1999). DOI: https://doi.org/10.1002/(SICI)1521-4095(199911)11:16<1365::AID-DMA1365>3.0.CO;2-F

[13] M. Miwa, A. Nakajima, A. Fujishima, K. Hashimoto, T. Watanabe, Effects of the Surface Roughness on Sliding Angles of Water Droplets on Superhydrophobic Surfaces. Langmuir **16**, 13, 5754-5760 (2000). DOI: https://doi.org/10.1021/la991660o

[14] A. Nakajima, K. Hashimoto, T. Watanabe, K. Takai, G. Yamauchi, A. Fujishima, Transparent Superhydrophobic Thin Films with Self-Cleaning Properties. Langmuir **16**, 17, 7044-7047 (2000). DOI: https://doi.org/10.1021/la000155k

[15] J. Bico, C. Marzolin, D. Quéré, Pearl drops, Europhys. Lett. **47**, 220- 226 (1999). DOI: https://doi.org/10.1209/epl/i1999-00453-y

[16] T. Onda, S. Shibuichi, N. Satoh, K. Tsujii, Super-Water-Repellent Fractal Surfaces. Langmuir **12**, 9, 2125-2127 (1996). DOI: https://doi.org/10.1021/la950418o_

[17] S. Shibuichi, T. Onda, N. Satoh, K. Tsujii, Super Water-Repellent Surfaces Resulting from Fractal Structure. J. Phys. Chem. **100**, 50, 19512-19517 (1996). DOI: https://doi.org/10.1021/jp9616728

[18] B. Yin, L. Fang, A. Tang, Q-L. Huang, J. Hu, J.-H. Mao, G. Bai, H. Bai, Novel strategy in increasing stability and corrosion resistance for super-hydrophobic coating on aluminum alloy surfaces. Appl. Surf. Sci. **258**, 580-585 (2011). DOI: https://doi.org/101016/japsusc201108063

[19] D.K Sarkar, M. Farzaneh, Superhydrophobic Coatings with Reduced Ice Adhesion. J. Adhes. Sci. Technol. **23**, 9, 1215-1237 (2009). DOI: https://doi.org/10.1163/156856109X433964

[20] D. Quéré, Non-sticking drops. Rep. Prog. Phys. **68**, 2495-2532 (2005). DOI: http://iopscience.iop.org/0034-4885/68/11/R01

[21] T. Kako, A. Nakajima, H. Irie, Z. Kato, K. Uematsu, T. Watanabe, K. Hashimoto, Adhesion and sliding of wet snow on a superhydrophobic surface with hydrophilic channels. J. Mater. Sci. **39**, 547-555 (2004).
DOI: https://doi.org/10.1023/B:JMSC.0000011510.92644.3fv

[22] M. F. Montemor, Functional and smart coatings for corrosion protection: A review of recent advances. Surf. Coat. Technol. **258**, 17-37, (2014).
DOI: https://doi.org/10.1016/j.surfcoat.2014.06.031

[23] A.M.A. Mohamed, A.M. Abdullah, N.A. Younan, Corrosion behavior of superhydrophobic surfaces: A review. Arabian J. Chem. **8**, 6, 749-765 (2015).
DOI: https://doi.org/10.1016/j.arabjc.2014.03.006

[24] P.C.R. Varma, P. Periyat, M. Oubaha, C. McDonagh, B. Duffy, Application of niobium enriched ormosils as thermally stable coatings for aerospace aluminum alloys. Surf. Coat. Technol. **205**, 3992-3998 (2011).
DOI: https://doi.org/10.1016/j.surfcoat.2011.02.023

[25] A.M. Abdel-Gaber, B.A. Abd-El-Nabey, I.M. Sidahmed, A.M. El-Zayady, M. Saadawy, Mater. Chem. Phys. **98**, 2-3, 291-297 (2006).
DOI: https://doi.org/10.1016/j.matchemphys.2005.09.023

[26] W.A. Badawy, F.M. Al-Kharafi, A.S. El-Azab, Electrochemical behaviour and corrosion inhibition of Al, Al-6061 and Al–Cu in neutral aqueous solutions. Corros. Sci. **41**, 709-727 (1999).
DOI: https://doi.org/10.1016/S0010-938X(98)00145-0

[27] B. Yin, L. Fang, J. Hu, A.Q. Tang, W.H. Wei, J. He, Preparation and properties of super-hydrophobic coating on magnesium alloy. Appl. Surf. Sci. **257**, 1666-1671 (2010).
DOI: https://doi.org/10.1016/j.apsusc.2010.08.119

[28] J. D. Brassard, D. K. Sarkar, J. Perron, et al., Nano-micro structured superhydrophobic zinc coating on steel for prevention of corrosion and ice adhesion. J. Colloid. Interface Sci. **447**, 240-7 (2015). DOI: https://doi.org/10.1016/j.jcis.2014.11.076

[29] Y. Huang, D.K. Sarkar, X.-G. Chen, Superhydrophobic nanostructured ZnO thin films on aluminum alloy substrates by electrophoretic deposition process. Appl. Surf. Sci. **327**, 327-334 (2015). DOI: https://doi.org/10.1016/j.apsusc.2014.11.170

[30] Y. Huang, D.K. Sarkar, X.-G. Chen, Fabrication of Superhydrophobic Surfaces on Aluminum Alloy Via Electrodeposition of Copper Followed by Electrochemical Modification. Nano-Micro Lett. **3**, 160-165 (2011).
DOI: https://doi.org/10.1007/BF03353667

[31] S. Pan, N. Wang, D. Xiong, Y. Deng, Y. Shi, Fabrication of superhydrophobic coating via spraying method and its applications in anti-icing and anti-corrosion. Appl. Surf. Sci **389**, 547-553 (2016).
DOI: https://doi.org/10.1016/j.apsusc.2016.07.138

[32] N. Hassan, M. M. Fadhali, S. Al-Sulaimi, et al., Development of sustainable superhydrophobic coatings on aluminum substrate using magnesium nanoparticles for enhanced catalytic activity, self-cleaning, and corrosion resistance. J. Mol. Liq. **383**, 122085 (2023). DOI: https://doi.org/10.1016/j.molliq.2023.122085

[33] R.G.C. da Silva, M. I.C. Malta, L. A.P. de Carvalho, et al., Low-cost superhydrophobic coating on aluminum alloy with self-cleaning and repellency to water-based mixed liquids for anti-corrosive applications. Surf. Coat. Technol. **457**, 129293 (2023).
DOI: https://doi.org/10.1016/j.surfcoat.2023.129293

[34] Z. Belamri, L. Boumaza, S. Boudjadar, Electroplating of hydrophobic/hydrophilic ZnO nano-structural coatings on metallic substrates. Phys. Scr. 98, 125949 (2023).
DOI: https://doi.org/10.1088/1402-4896/ad0a2a

[35] Z. Belamri, W. Darenfad, N. Guermat, Impact of Annealing Temperature on Surface Reactivity of ZnO Nanostructured Thin Films Deposited on Aluminum Substrate. J. Nano-Electron. Phys. **15**, 02026 (2023). DOI: https://doi.org/10.21272/jnep.15(2).02026

[36] E.Z. Alejandre, J.A.C. Martinez, A.R. Garibo, L.P. Arrietaal, Structural, electrical and optical properties of indium chloride doped ZnO films synthesized by Ultrasonic Spray Pyrolysis technique. Thin Solid Films **524**, 44-49 (2012).
DOI: http://dx.doi.org/10.1016/j.tsf.2012.09.050

[37] Z.N. Kayani, M. Sahar, S. Riaz, S. Naseem, Z. Saddiqe, Enhanced magnetic, antibacterial and optical properties of Sm doped ZnO thin films: Role of Sm doping. Opt. Mater. **108**, 110457 (2020).
DOI: https://doi.org/10.1016/j.optmat.2020.110457

[38] R. Aydin, B. Sahin, Comprehensive research on physical properties of Zn and M (M: Li, Na, K) double doped cadmium oxide (CdO) nanostructures using SILAR method. Ceram. Int. **43**, 12, 9285-9290 (2017).
DOI: https://doi.org/10.1016/j.ceramint.2017.04.087

[39] B. Sahin, T. Kaya, Facile preparation and characterization of nanostructured ZnO/CuO composite thin film for sweat concentration sensing applications. Mater. Sci. Semicond. Process. **121**, 105428 (2021). DOI: https://doi.org/10.1016/j.mssp.2020.105428

[40] D. Kwon, D. Kang, E. Yeom, Impact and boiling characteristics of an impinging ethanol drop on a heated Al alloy surface. Int. J. Heat. Mass. Transfer. **169**, 120927 (2021)
DOI: https://doi.org/10.1016/j.ijheatmasstransfer.2021.120927

[41] K.L. Foon, M. Kashif, U. Hashim, Wei-Wen Liu, Effect of different solvents on the structural and optical properties of zinc oxide thin films for optoelectronic applications. Ceram. Int. **40**, 753-761 (2014). DOI: https://doi.org/10.1016/j.ceramint.2013.06.065

[42] Y.-C. Wu, Y.-C. Tai, Effects of alcohol solvents on anatase TiO_2 nanocrystals prepared by microwave-assisted solvothermal method. J. Nanopart. Res. **15**, 1-11 (2013).
DOI: https://doi.org/10.1007/s11051-013-1686-2J

[43] O. Wiranwetchayan, S. Promnopas, T. Thongtem, A. Chaipanich, S. Thongtem, Effect of alcohol solvents on TiO2 films prepared by sol–gel method. Surf Coat Technol **326**, A, 310-315 (2017).
DOI: https://doi.org/10.1016/j.surfcoat.2017.07.068

[44] N. Talebian, M. Kheiri, Sol gel derived nanostructured nickel oxide films: Effect of solvent on crystallographic orientations. Solid. State. Sci. **27**, 79-83 (2014).
DOI: https://doi.org/10.1016/j.solidstatesciences.2013.11.010

[45] A. Marty, S. Andrieu, Croissance et structure des couches minces. Colloque C7, supplément au Journal de Physique III, Vol. 6, novembre, C7-11 (1996).

[46] T.J. Coutts, D.L. Young, X. Li, Characterization of Transparent Conducting Oxides. MRS Bulletin **25** (8), 58-65 (2000).
DOI: https://doi.org/10.1557/mrs2000.152

[47] M. Chen, Z.L. Pei, C. Sun, L.S. Wen, X. Wang, Surface characterization of transparent conductive oxide Al-doped ZnO films. Journal of Crystal Growth **220**, 254-262 (2000). DOI: https://doi.org/10.1016/S0022-0248(00)00834-4

[48] E.S. Tüzemen, S. Eker, H. Kavak, R. Esen, Dependence of film thickness on the structural and optical properties of ZnO thin films. Appl. Surf. Sci. **255**, 6195-6200 (2009). DOI: https://doi.org/10.1016/j.apsusc.2009.01.078

[49] T. Srinivasulu, K. Saritha, K.T. Ramakrishna Reddy, Synthesis and characterization of Fe-doped ZnO thin films deposited by chemical spray pyrolysis. Modern Electronic Materials **3**, 2, 76-85 (2017). DOI: https://doi.org/10.1016/j.moem.2017.07.001

[50] T.C. Damen, S.P.S. Pqrtq, B. Tell, Raman Effect in Zinc Oxide. Phys. Rev. **142**, 2, 570-574 (1966). DOI: https://doi.org/10.1103/PhysRev.142.570_

[51] R. Taziwa, E. Meyer, D. Katwire, L. Ntozakhe, Influence of Carbon Modification on the Morphological, Structural, and Optical Properties of Zinc Oxide Nanoparticles Synthesized by Pneumatic Spray Pyrolysis Technique. J. Nanomater. Article ID 9095301, 1-11, (2017). DOI: https://doi.org/10.1155/2017/9095301

[52] C. Justin Raj, R.K. Joshi, K.B.R. Varma, Synthesis from zinc oxalate, growth mechanism and optical properties of ZnO nano/micro structures. Cryst. Res. Technol. **46**, 11, 1181-1188 (2011). DOI: https://doi.org/10.1002/crat.201100201

[53] M. Silambarasan, S. Saravanan, T. Soga, Raman and Photoluminescence Studies of Ag and Fe-doped ZnO Nanoparticles. Int. J. Chem. Tech. Res. **7** (3), 1644-1650 (2015)

[54] J.F. Jurado, A. Londono-Calderon, F.F. Jurado-Lasso, J.D. Romero-Salazar, Influence of the precursors in the morphology, structure, vibrational order and optical gap of nanostructured ZnO. Revista Mexicana de Fisica **60**, 296-300 (2014).

[55] N.J. Shirtcliffe, G. McHale, M.I. Newton, C.C. Perry, Wetting and wetting transitions on copper-based superhydrophobic surfaces. Langmuir **21**, 937-43 (2005). DOI: https://doi.org/10.1021/la048630s

[56] L. Gao, T.J. McCarthy, The "lotus effect" explained: two reasons why two length scales of topography are important. Langmuir **22**, 2966-67 (2006). DOI: https://doi.org/10.1021/la0532149

[57] B. Bhushan, Y.C. Jung, Micro- and nanoscale characterization of hydrophobic and hydrophilic leaf surfaces. Nanotechnology **17**, 2758-72 (2006). DOI: http://dx.doi.org/10.1088/0957-4484/17/11/008

[58] M. Nosonovsky, Multiscale roughness and stability of superhydrophobic biomimetic interfaces. Langmuir **23**, 3157-61 (2007). DOI: https://doi.org/10.1021/la062301d

[59] L. Gao, T.J. McCarthy, A commercially available perfectly hydrophobic material. Langmuir **23**, 9125-27 (2007). DOI: https://doi.org/10.1021/la701097k

[60] R. Wang, K. Hashimoto, A. Fujishima, et al., Photogeneration of highly amphiphilic TiO_2 surfaces. Adv. Mater. **10**, 135-38 (1999). DOI: https://doi.org/10.1002/(SICI)1521-4095(199801)10:2<135::AID-ADMA135>3.0.CO2-M

[61] P.P.K. Smith, B.G. Hyde, The homologous series Sb_2S_3.*n*PbS: structures of diantimony dilead pentasulphide, $Pb_2Sb_2S_5$, and the related phase diantimony ditin pentasulphide. $Sn_2Sb_2S_5$, Acta Crystallogr. Sec. C **39**, 1498-1502 (1983). DOI: https://doi.org/10.1107/S0108270183009038

[62] T.P. Rao, M.C.S. Kumar, Effect of thickness on structural, optical and electrical properties of nanostructured ZnO thin films by spray pyrolysis. Appl. Surf. Sci. **255**, 4579-4584 (2009). DOI: https://doi.org/10.1016/j.apsusc.2008.11.079

[63] J.C. Lodder, T. Wielinga, J. Worst, R.f.-sputtered Co-Cr layers for perpendicular magnetic recording I: Structural properties. Thin Solid Films **101**, 61-73 (1983). DOI: https://doi.org/10.1016/0040-6090(83)90493-5

[64] S. Benramache, B. Benhaoua, N. Khechai, F. Chabane, Elaboration et caractérisation des couches minces de ZnO. Materiaux Tech. **100**, 573-580 (2012). DOI: https://doi.org/10.1051/mattech/2012052

[65] S.A. Khan, F. Al-Hazmi, S. Al-Heniti, A. Faidah, A. Al-Ghamdi, Effect of cadmium addition on the optical constants of thermally evaporated amorphous Se–S–Cd thin films Curr. Appl. Phys. **10**, 145-152 (2010). DOI: https://doi.org/10.1016/j.cap.2009.05.010

[66] G. Kenanakis, E. Stratakis, K. Vlachou, D. Vernardou, E. Koudoumas, N. Katsarakis, light-induction reversible hydrophylicity of ZnO structures grown by aqueous chemical growth. Appl. Surf. Sci. **254**, 5695-5699 (2008). DOI: https://doi.org/10.1016/j.apsusc.2008.03.055

[67] J. Lv, J. Zhu, K. Huang, F. Meng, X. Song, Z. Sun, Tunable surface wettability of ZnO nanorods prepared by two-step method. Appl. Surf. Sci. **257**, 7534-7538 (2011). DOI: https://doi.org/10.1016/j.apsusc.2011.03.113

[68] R.R. Cranston, H.L. Benoît, Metal phthalocyanines: thin-film formation, microstructure, and physical properties. RSC Adv. **11**, 21716-21737 (2021). DOI: https://doi.org/10.1039/d1ra03853b

[69] J. Zhang, W. Huang, T. Han, Wettability of Zinc Oxide Surfaces with Controllable Structures. Langmuir **22**, 2946-2950 (2006). DOI: https://doi.org/10.1021/la053428q

[70] Y. Huang, D.K. Sarkar, X.-G. Chen, Fabrication of Superhydrophobic Surfaces on Aluminum Alloy Via Electrodeposition of Copper Followed by Electrochemical Modification. Nano-Micro Lett. **3**, 160-165 (2011). DOI: https://doi.org/10.1007/BF03353667

[71] D.K. Sarkar, M. Farzaneh, R.W. Paynter, Superhydrophobic properties of ultrathin rf-sputtered Teflon films coated etched aluminum surfaces. Mater. Lett. **62**, 1226-1229 (2008). DOI: https://doi.org/10.1016/j.matlet.2007.08.051

[72] A.B.D. Cassie, S. Baxter, Wettability of porous surfaces. Trans. Faraday Soc. **40**, 546 (1944). DOI: https://doi.org/10.1039/TF9444000546

[73] T. Liu, S. Chen, S. Cheng et al., Corrosion behavior of superhydrophobic surface on copper in seawater. Electrochimica Acta **52**, 8003-8007 (2007). DOI: https://doi.org/10.1016/j.electacta.2007.06.072